12th ANKARA INTERNATIONAL AEROSPACE CONFERENCE **AIAC-2023-028**
13-15 September 2023 - Online, Ankara, TURKEY

DEFECT SENSITIVITY STUDY ON 3-D PRINTED AUXETIC TUBULAR STRUCTURES

Ismail Safa Karaca*
Middle East Technical University
Turkish Aerospace Industries Inc.
Ankara, Turkey

Ercan Gürses †
Middle East Technical University
Ankara, Turkey

ABSTRACT

Due to their unique features, auxetic materials are gaining attraction from structural engineers. Auxetic materials uncustomarily squeeze and expand under compressive and tensile forces, respectively. With this superior feature, their structures can be used in many applications, such as health technologies, the aerospace industry, and nanotechnologies. Auxetic structures are mostly manufactured by additive manufacturing because of their complex shapes. However, additive manufacturing has its inherent complications. 3-D printing and post-processing may cause defects in the parts. In this study, the sensitivity of the auxetic structures to some defect types is studied. Considering these predetermined sensitivities, some preliminary manufacturing guides are designated.

INTRODUCTION

Auxetic structures have negative Poisson's Ratios. They expand (shrink) laterally when longitudinally pulled (compressed). Because of this feature, they have a high potential for use in medical applications, protective devices, smart sensors and filters, auxetic fasteners, and textiles, as mentioned in [Ren et al., 2018a]. In [Liu et al., 2021], an auxetic flexible stent was suggested as a potential application in treating tracheobronchial stenosis, which is the narrowing of the airways. In the aerospace industry, auxetic materials have areas of utilization as sensors, protective devices, or fasteners. In [Ren et al., 2018b], auxetic nails were designed and analyzed to fasten wooden structures. Also, 3-D printed auxetic fasteners were studied in [Peel and Abdelrahman, 2012]. They showed that auxetic fasteners have superior properties to standard ones. A novel peanut-shaped structure is suggested, tested, and analyzed to compare the auxetic and stiffness characteristics of auxetic tubular structures in [Zhang et al., 2021]. The peanut-shaped structure is a valuable alternative to chiral-type and re-entrant structures, but it has difficulties in manufacturing by conventional methods. 3-D printing can ease the manufacturing of peanut-shaped structures, but some defects can be generated after additive processes. Therefore, in this study, the effects of these defects are investigated. Analyses are conducted to compare a peanut-shaped model with an ellipse-shaped

*M.S. Student in Department of Aerospace Engineering and Design Engineer in Department of Aerostructures, Email: safa.karaca@metu.edu.tr
†Assoc. Prof. in the Department of Aerospace Engineering, Email: gurses@metu.edu.tr

model with the same porosity and similar auxetic properties. Unit geometries of the peanut and ellipse shapes are demonstrated in Figure 1.

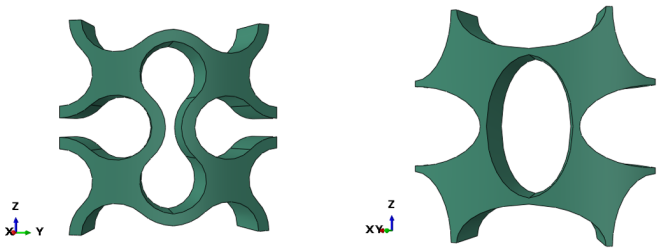
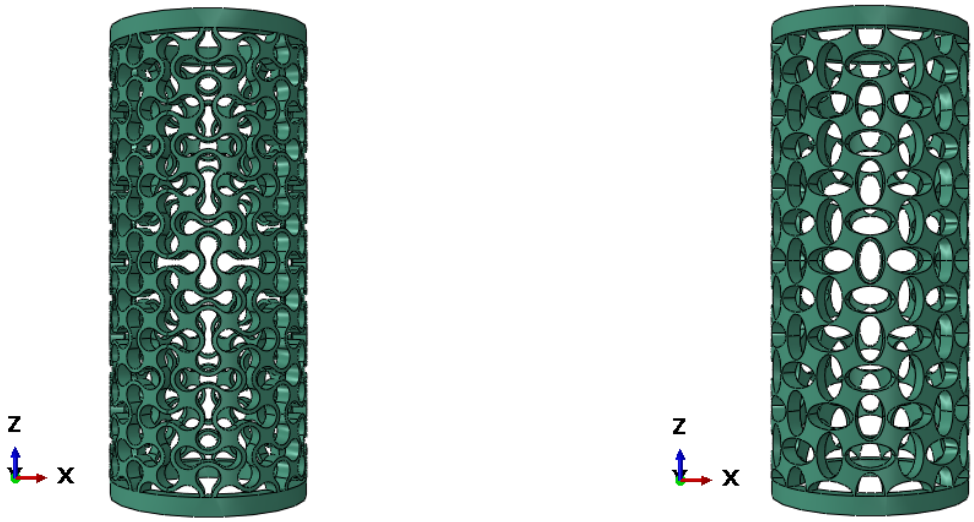


Figure 1: Unit geometries of peanut and ellipse-shaped auxetic structures

METHOD

This study analyzes the sensibility of auxetic structures to certain types of defects. As a finite element solver, Abaqus/Standart is used [ABAQUS, 2014]. The analyses are completed for four kinds of faults and two textures. First, faultless structures are analyzed, and their auxetic properties are determined. Faultless tubular structures are shown in Figure 2.



(a) Peanut-shaped tubular structure (b) Ellipse-shaped tubular structure

Figure 2: Faultless structures

Dimensions of the bodies and the material properties are the same as in the referred article [Zhang et al., 2021]. Its height is 130 mm, its outer diameter is 54.93 mm, and its inner diameter is 46.93 mm. So the thickness of the cylindrical shape is 4 mm. In all faultless and defective geometries, the height of the cylinder is through the z-direction, and the cylinder's cross-section is in the xy-plane. The Young Modulus of the base material is 1.114 GPa, and Poisson's Ratio is 0.413.

In these structures, four different types of defects are created. In the first defect, the printer is assumed to drain off additional material. So, some holes can not emerge. In the parts, one-hole and linearly aligned several defects are considered. The one-hole defect is placed on the third horizontal level from the bottom. Its radial position is not significant due to the radial symmetry of the body. Then the number of defective holes increased from 1 to 16. In the radial direction, there are eight units and sixteen holes, so in the last step, all holes of a horizontal line are filled. Furthermore, another horizontal line defect is considered on the sixth level from the bottom. In addition, one vertical line defect is implemented at a random radial position, and the defective hole number is increased from 1 to 12 again. Base defective tubular structures of this type of defect are shown in Figure 3 and Figure 4.

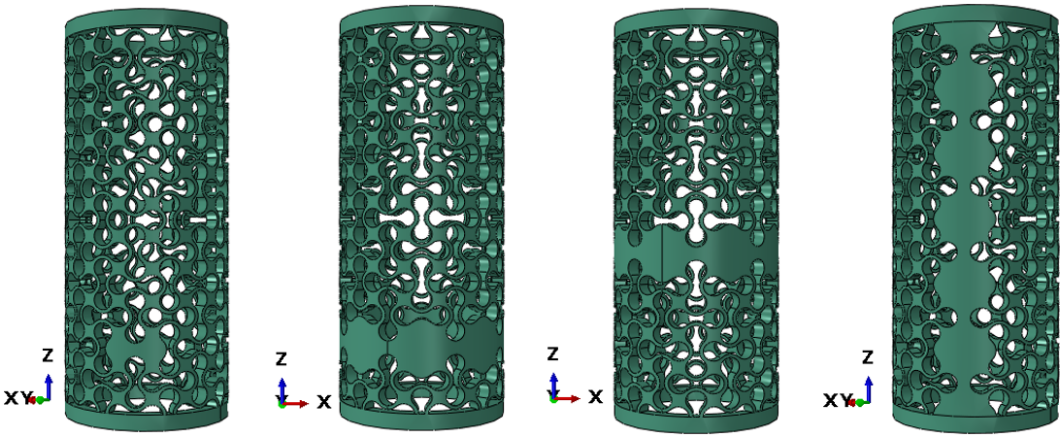


Figure 3: Defective peanut-shaped bodies (Left to right: one-hole, lower horizontal line, upper horizontal line, vertical line defects)

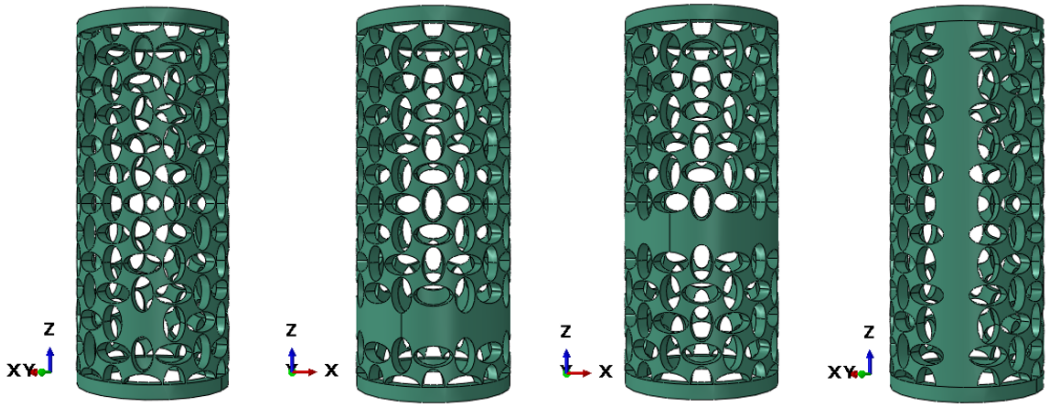


Figure 4: Defective ellipse-shaped bodies (Left to right: one-hole, lower horizontal line, upper horizontal line, vertical line defects)

The second defect originated from the retraction fault of printers. Especially in filament-based printers, while a layer is printing and encounters a hole, filaments must be retracted from the nozzle and fed out again after the gap. If the geometry has many holes and the printer lacks enough capability, it can not print the legs of these holes smoothly, and these regions can not be loaded in compression or tension forces. In [Bas et al., 2019], extrusion interruption, deformation on the side surfaces, and oozing are examples of the retraction fault. This defect is modeled in the peanut and ellipse shapes, as shown in Figures 5 and 6, respectively. Again these defects are translated along horizontal and vertical lines. There are two different horizontal lines created same as the previous defect type. Also, in the horizontal line, defects are applied from 1 unit to 4 units, and in the vertical line, from 1 unit to 6 units.

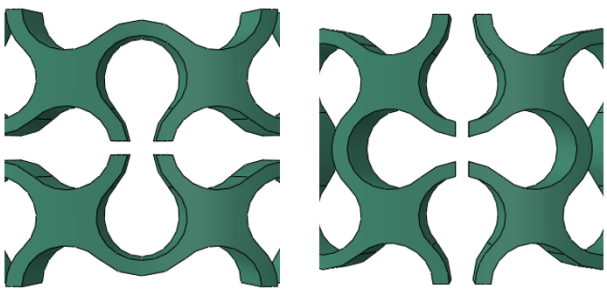


Figure 5: Defective peanut-shaped unit (Left: horizontal line defect, right: vertical line defect)

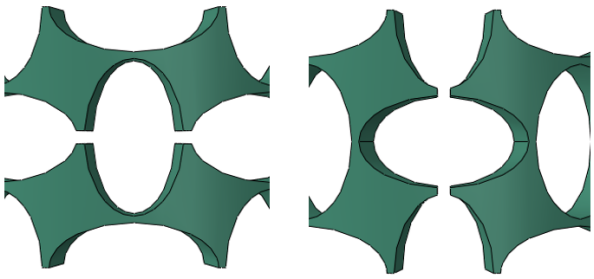


Figure 6: Defective ellipse-shaped unit (Left: horizontal line defect, right: vertical line defect)

As mentioned in [Krčma and Paloušek, 2019], geometries have large curvatures that can be deformed while printing. They suggested that 5-axis nozzles should be used while printing this kind of geometry. Some support structures can also be added for creating peanut and ellipse shapes. However, these two methods are expensive and challenging for manufacturing. For analyzing the effect of this defect on Poisson's Ratio of hole structure, units shown in Figures 7 and 8 are modeled for peanut-shaped and ellipse-shaped structures, respectively.

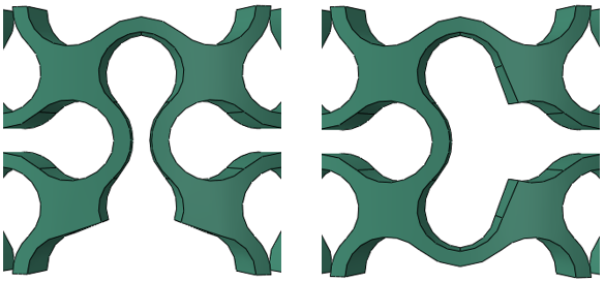


Figure 7: Defective peanut-shaped unit (Left: horizontal line defect, right: vertical line defect)

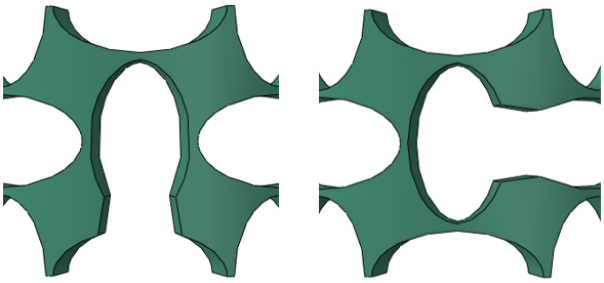


Figure 8: Defective ellipse-shaped unit (Left: horizontal line defect, right: vertical line defect)

The elephant foot fault inspires the last modeled defect. It occurs due to insufficient cooling, an unleveled platform, or a nozzle as defined in [Bas et al., 2019]. The horizontal effect of this defect is different diameters between lower and upper surfaces. In nominal design, the diameter of the inner surface is 46.93 mm, and the diameter of the outer surface is 54.93 mm. In the defective geometries, the outer diameter of the lower surface is bigger than the nominal diameter, and the inner diameter of the lower surface is smaller than the nominal diameter. On the upper surface, the outer is smaller, and the inner is bigger. The differences between the nominal diameter and the defective diameter of the inner and outer surfaces of the upper and the lower surfaces are equal. Visualization of the difference between nominal and defective geometries of the peanut-shaped and ellipse-shaped bodies is given in Figure 9. The diameter differences of the viewed geometries are 2 mm. It means that the outer diameter of the lower surface is 56.93 mm, and the inner diameter of the lower surface is 44.93 mm. So, the wall thickness of the lower surface is 6 mm in this sample.

Also, The outer diameter of the upper surface is 52.93 mm, and the inner diameter is 48.93 mm. On the upper surface, the wall thickness is 2 mm.

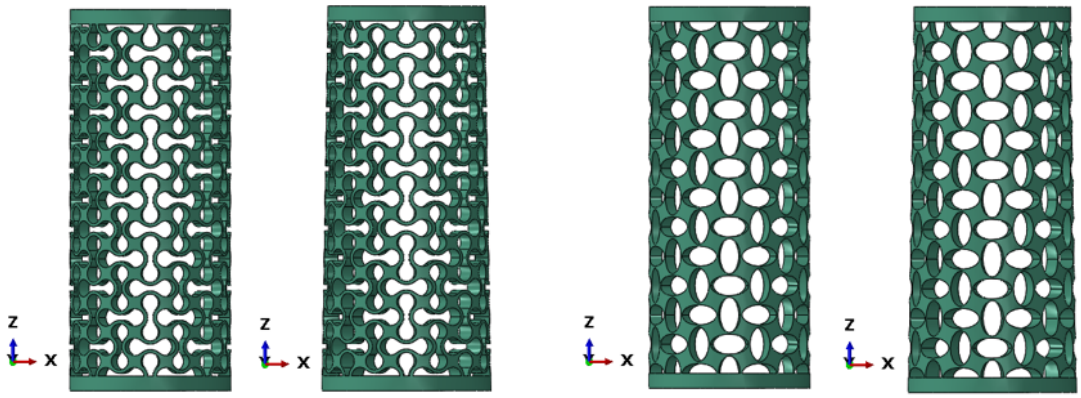


Figure 9: Nominal and defective bodies (Left: peanut-shaped geometry, right: ellipse-shaped geometry)

The vertical effect of the last defect is modeled as a not perfectly circular cross-section. If the 3d printing program prints the body perpendicular to the x-z plane (in the direction of the y-axis), the cross-section in the x-y plane may not be a perfect circle. It is assumed that the cross-section is shaped after printing as an ellipse, and its major and minor axes differ a value from the nominal circle diameter. In Figure 10, 2 mm differed geometry is shown for defective geometry. It is a visualization of the peanut-shaped geometry, but the view is the same for the ellipse-shaped geometry. The major axis of the shown cross-section is 2 mm bigger than the nominal diameter, and the minor axis is 2 mm smaller.

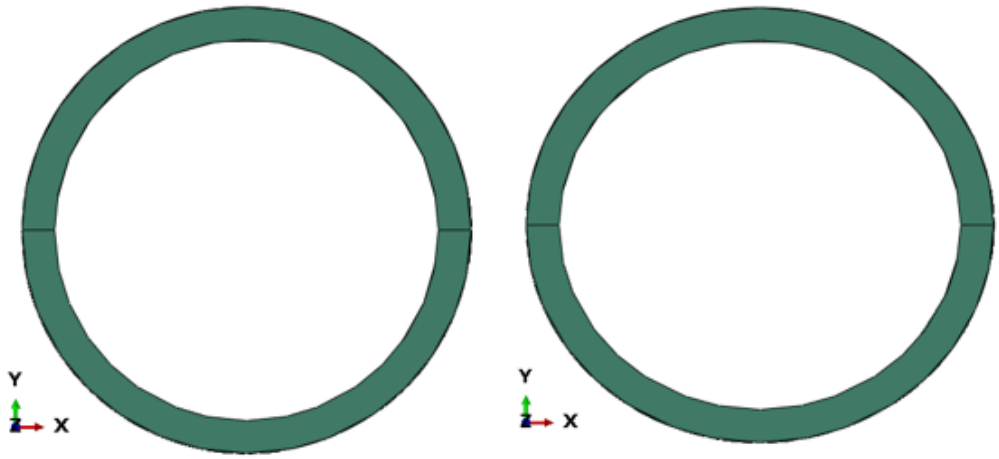
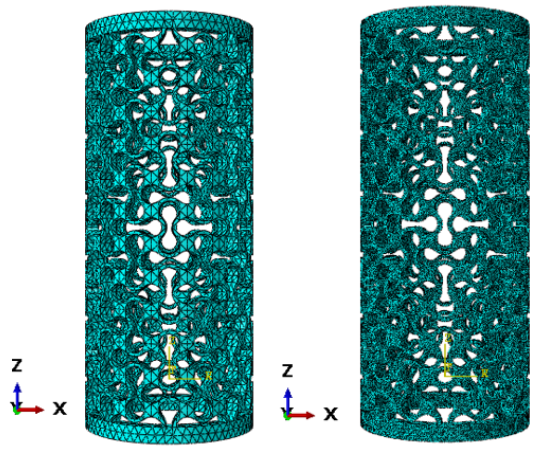


Figure 10: Nominal and defective bodies for peanut-shaped and ellipse-shaped geometries

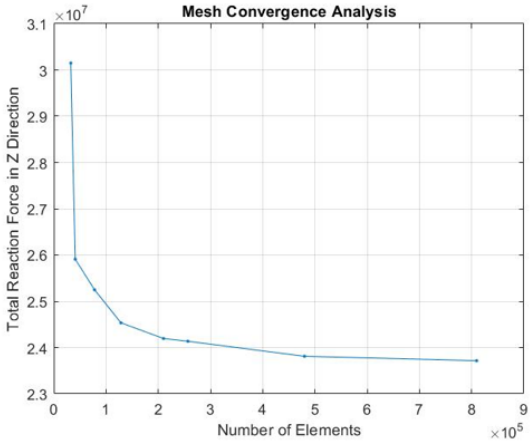
All analyses apply a 1 mm compressive displacement in the axial direction through the top of the structure. The angular displacements of the bottom and top surfaces are set to zero to prevent rigid body rotations. Also, the lower surface is fixed in the axial z-direction. Boundary conditions are shown in Figure 12a. In all models, the same boundary conditions are used.

Perfect peanut-shaped geometry is filled with eight different mesh intensities and analyzed to decide the proper mesh size. Views of the coarsest mesh and the finest mesh can be seen in Figure 11a, and the result of the mesh study can be seen in Figure 11b. In the graph, the y-axis depicts the total reaction forces on the lower surface in the z-direction, and the x-axis shows the number of elements.

According to this graph, the 256844 element for this body is enough for an accurate calculation. So, the approximate element size is 1 mm for an accurate FEM calculation. Then, in perfect peanut-shaped and ellipse-shaped bodies, there are 256844 and 253968 elements, respectively. Element type C3D10 (10-noded tetrahedron with full integration) is selected for all geometries. Meshed geometries are depicted in Figure 12b and Figure 12c.

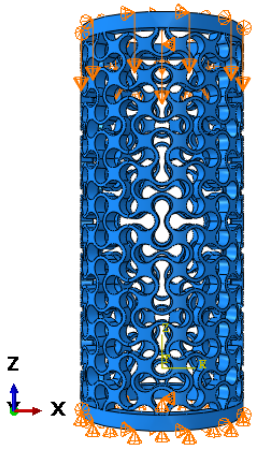


(a) Examples of low and high mesh intensities: 32561 elements (left), 809694 elements (right)

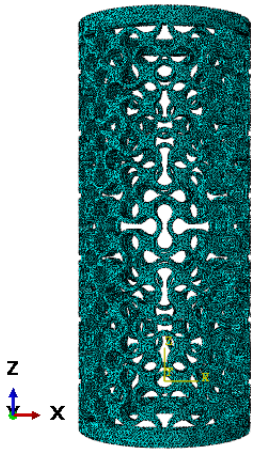


(b) Change of total reaction force in the base in the z-direction with increasing element numbers

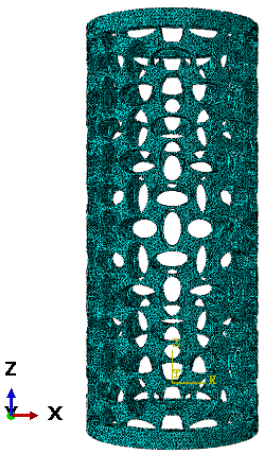
Figure 11: A coarse and a fine mesh for peanut-shaped geometry and the result of the mesh Study



(a) Boundary condition of peanut-shaped structure



(b) Meshed geometry of peanut-shaped body (256844, C3D10 elements)



(c) Meshed geometry of ellipse-shaped body (253968, C3D10 elements)

Figure 12: BC on peanut-shaped geometry (At z=0 mm: no BC on radial direction, fixed BC on angular direction, fixed BC on z direction. At z=130 mm: no BC on radial direction, fixed BC on angular direction, -1 mm deflection BC on z direction.) and meshed geometries of both geometry

For lower computational costs, the NLGEOM Function (Non-Linear Geometry Function) of ABAQUS/-Standart is disabled for the analyses. Even if this function is disabled, results are reasonable when strain levels are less than 1 percent. The difference between NLGEOM ON and OFF options is given in Table 1. In the table, reaction forces on the bodies for NLGEOM ON and OFF can be seen. The difference values are in percentages, and the units of force and deflection are Newtons

and millimeters, respectively. It is clear that error increases with increasing deflection, but at 1 mm deflection, it is just 1.77 percent.

Table 1: Total reaction forces with different prescribed displacement values for NLGEOM ON and OFF options

DISPLACEMENT	NLGEOM OFF	NLGEOM ON	DIFFERENCE
0.50 mm	8.30×10^1 N	8.23×10^1 N	0.88
1.00 mm	1.66×10^2 N	1.63×10^2 N	1.77
1.50 mm	2.49×10^2 N	2.42×10^2 N	2.66
2.00 mm	3.32×10^2 N	3.21×10^2 N	3.56
5.00 mm	8.30×10^2 N	7.61×10^2 N	9.09

Poisson's ratio is calculated by finding the mean radial strain of the outer surface nodes at the auxetic region and dividing it by the strain in the compressed direction. Auxetic areas refer to the volume between two upper and lower rings where the peanut and ellipse shapes are located.

RESULTS AND DISCUSSION

Von Mises stresses and radial displacements of the models are depicted in Figure 13. Moreover, porosity values (ϕ), radial strain values (ϵ_r), Poisson's ratios, maximum Von-Mises stresses (σ_v), and reaction forces (RF_z) can be seen in Table 2. From the table, Poisson's ratios of the models are the same, but their reaction forces in the z-direction are different. The ellipse reacts approximately four times higher than the peanut shape to 1 mm of compressive displacement. Moreover, the maximum Von Mises stress value of the peanut shape is about a quarter of the ellipse's maximum Von Mises stress value. Therefore, according to the auxetic property-to-stiffness ratio, the peanut shape is more effective than the ellipse. These results show similarities with the results of [Zhang et al., 2021]. The Poisson's ratio of the peanut shape was calculated as -0.754 in that study, and the value of the ellipse model was similar. Also, the maximum Von Mises stresses ratio between the peanut shape and ellipse models is approximately 0.25, but their values are higher because of different compressive displacements. They found the maximum Von Mises stress of the peanut shape and ellipse models in 5 mm displacement as $19.871 \times 10^6 Pa$, and $78.011 \times 10^6 Pa$, respectively.

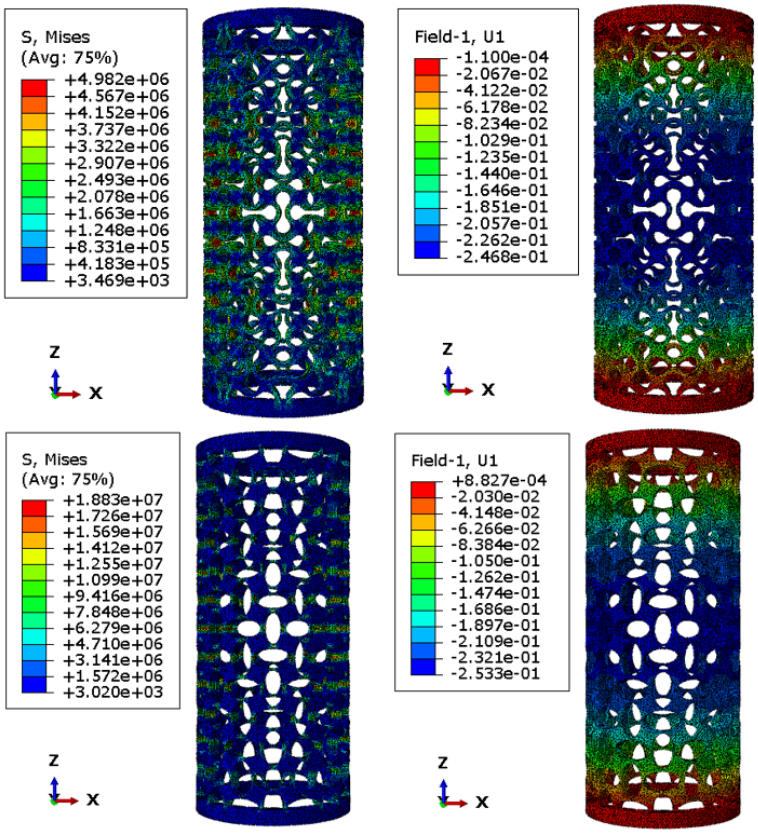


Figure 13: Stress and radial displacement results (In left-top Von-Mises Stress result of peanut-shaped structure, in right-top radial displacement result of the peanut-shaped structure, in right-bottom Von-Mises Stress result of ellipse-shaped structure, in left-bottom radial displacement result of ellipse-shaped structure)

Table 2: Results of perfect structures

Models	ϕ	ϵ_r	ν_{zr}	max. σ_v (Pa)	RF_z (N)
Peanut shape	0.66	-6.08×10^{-3}	-0.73	4.98×10^{6}	2.41×10^{1}
Ellipse	0.66	-6.12×10^{-3}	-0.73	1.88×10^{7}	9.22×10^{1}

Results of defect sensitivity analyses are shown in Table 3 and Table 4 for the filled holes in a horizontal line defect. In both shapes, the auxetic property is decreasing, and the reaction force in the base is increasing while the number of defective holes is increasing. Both geometries are affected by this type of defect at the same rate.

Table 3: Results of peanut-shaped structures for the first type of defect in a lower horizontal line (Perfect and defectives)

Models	ν_{zr}	RF_z (N)
No Defect	-0.73	2.41×10^{1}
1 hole	-0.72	2.57×10^{1}
3 holes	-0.71	2.63×10^{1}
5 holes	-0.70	2.72×10^{1}
7 holes	-0.69	2.80×10^{1}
16 holes	-0.63	3.10×10^{1}

Table 4: Results of ellipse-shaped structures for the first type of defect in a lower horizontal line (Perfect and defectives)

Models	ν_{zr}	RF_z (N)
No Defect	-0.73	9.22×10^{1}
1 hole	-0.72	9.91×10^{1}
3 holes	-0.71	1.04×10^{2}
5 holes	-0.70	1.08×10^{2}
7 holes	-0.68	1.12×10^{2}
16 holes	-0.63	1.26×10^{2}

Results of the same defect applied to an upper level of horizontal lines can be shown in Tables 5 and 6 for peanut-shaped and ellipse-shaped geometries, respectively. The same conclusions with the lower line can be made, but in this case, both auxetic property and reaction force is affected more. It is an outcome of boundary conditions. Because the lower defect line is closer than the upper line to the boundaries, the effect of the lower line is small.

Table 5: Results of peanut-shaped structures for the first type of defect in a middle horizontal line (Perfect and defectives)

Models	ν_{zr}	RF_z (N)
No Defect	-0.73	2.41×10^1
1 holes	-0.72	2.62×10^1
3 holes	-0.70	2.81×10^1
5 holes	-0.67	2.99×10^1
7 holes	-0.65	3.16×10^1
16 hole	-0.58	3.81×10^1

Table 6: Results of ellipse-shaped structures for the first type of defect in a middle horizontal line (Perfect and defectives)

Models	ν_{zr}	RF_z (N)
No Defect	-0.73	9.22×10^1
1 hole	-0.71	1.07×10^2
3 holes	-0.69	1.17×10^2
5 holes	-0.67	1.27×10^2
7 holes	-0.64	1.37×10^2
16 holes	-0.57	1.71×10^2

When the part is manufactured on the xy-plane (z-direction), defects may be in the vertical lines. So, the results of the vertical line of the first defect are viewed in Tables 7 and 8 for peanut and ellipse geometries. It is clear that the auxetic property is decreasing while the number of filled holes is increasing, but the auxetic property of the peanut-shaped geometry is slightly less sensitive to this type of vertical defect. In terms of reaction force, the peanut-shaped model is affected substantially more, but also reaction forces in the ellipse-shaped model increase with the number of defective holes.

Table 7: Results of peanut-shaped structures for the first type of defect in a vertical line (Perfect and defectives)

Models	ν_{zr}	RF_z (N)
No Defect	-0.73	2.41×10^1
2 holes	-0.72	2.57×10^1
4 holes	-0.71	2.90×10^1
8 holes	-0.64	5.07×10^1
12 holes	-0.58	2.60×10^2

Table 8: Results of ellipse-shaped structures for the first type of defect in a vertical line (Perfect and defectives)

Models	ν_{zr}	RF_z (N)
No Defect	-0.73	9.22×10^1
2 holes	-0.72	9.97×10^1
4 holes	-0.70	1.15×10^2
8 holes	-0.62	2.00×10^2
12 holes	-0.55	4.66×10^2

Peanut-shaped and ellipse-shaped models are affected at the same rate by horizontal defects, but the ellipse-shaped model is less sensitive to the first type of vertical defect than peanut-shaped in terms of the reaction forces. Suppose this defect is expected from a printer. In that case, both the peanut-shaped and ellipse-shaped models should be printed through the z-direction because the vertical defects affect the reaction force behavior of the bodies excessively. Poisson's Ratio is decreasing in both cases, so there can not an inference from auxetic property.

As a result of retraction fault, the second type of defect is analyzed. Results of the Poisson's ratio and reaction forces in the z-direction of lower horizontal line defective units can be seen in Tables 9 and 10 for peanut-shaped and ellipse-shaped models. Again, the auxetic property decreases with the number of defects, but in this case, reaction forces are decreasing because of separated units. Decreasing auxetic properties and reaction forces of the peanut-shaped model is more significant than the ellipse-shaped model, so we can say the peanut is more sensitive than the ellipse in this case.

Table 9: Results of peanut-shaped structures for the second type of defect in a lower horizontal line (Perfect and defectives)

Models	ν_{zr}	RF_z (N)
No Defect	-0.73	2.41×10^1
1 unit	-0.69	2.28×10^1
2 units	-0.63	2.09×10^1
3 units	-0.56	1.84×10^1
4 units	-0.48	1.57×10^1

Table 10: Results of ellipse-shaped structures for the second type of defect in a lower horizontal line (Perfect and defectives)

Models	ν_{zr}	RF_z (N)
No Defect	-0.73	9.22×10^1
1 unit	-0.72	8.92×10^1
2 units	-0.67	8.33×10^1
3 units	-0.61	7.49×10^1
4 units	-0.53	6.49×10^1

Results of the middle line of the second defect type are given in Tables 11 and 12 for peanut and ellipse models. Again, because of the boundary conditions, upper-line defects affect more.

Table 11: Results of peanut-shaped structures for the second type of defect in the middle horizontal line (Perfect and defectives)

Models	ν_{zr}	RF_z (N)
No Defect	-0.73	2.41×10^1
1 unit	-0.68	2.25×10^1
2 units	-0.59	1.97×10^1
3 units	-0.50	1.66×10^1
4 units	-0.41	1.36×10^1

Table 12: Results of ellipse-shaped structures for the second type of defect in the middle horizontal line (Perfect and defectives)

Models	ν_{zr}	RF_z (N)
No Defect	-0.73	9.22×10^1
1 unit	-0.71	8.86×10^1
2 units	-0.65	8.04×10^1
3 units	-0.56	6.95×10^1
4 units	-0.47	5.82×10^1

The vertical defect outcomes of this case are given in Tables 13 and 14 for peanut-shaped and ellipse-shaped bodies. According to these results, the retraction fault does not affect the auxetic property and stiffness of the body majorly.

Table 13: Results of peanut-shaped structures for the second type of defect in a vertical line (Perfect and defectives)

Models	ν_{zr}	RF_z (N)
No Defect	-0.73	2.41×10^1
1 unit	-0.72	2.39×10^1
2 units	-0.70	2.37×10^1
4 units	-0.71	2.35×10^1
6 units	-0.69	2.32×10^1

Table 14: Results of ellipse-shaped structures for the second type of defect in a vertical line (Perfect and defectives)

Models	ν_{zr}	RF_z (N)
No Defect	-0.73	9.22×10^1
1 unit	-0.73	9.16×10^1
2 units	-0.72	9.12×10^1
4 units	-0.71	9.03×10^1
6 units	-0.69	8.94×10^1

From the results, if the printer has the potential to do the second type of defect, both bodies should be printed through the z-direction. As horizontal defects significantly impact both auxetic and reaction force behavior.

Results of the third defect are given in Tables 15, 17, 19 for peanut geometry, and 16, 18, 20 for ellipse geometry for horizontal lower level, horizontal middle level and vertical defects.

Table 15: Results of peanut-shaped structures for the third type of defect in the lower horizontal line (Perfect and defectives)

Models	ν_{zr}	RF_z (N)
No Defect	-0.73	2.41×10^1
1 unit	-0.73	2.41×10^1
2 units	-0.73	2.40×10^1
3 units	-0.73	2.39×10^1
4 units	-0.73	2.39×10^1
8 units	-0.73	2.36×10^1

Table 16: Results of ellipse-shaped structures for the third type of defect in the lower horizontal line (Perfect and defectives)

Models	ν_{zr}	RF_z (N)
No Defect	-0.73	9.22×10^1
1 unit	-0.74	9.19×10^1
2 units	-0.74	9.17×10^1
3 units	-0.74	9.14×10^1
4 units	-0.74	9.12×10^1
8 units	-0.75	9.02×10^1

Table 17: Results of peanut-shaped structures for the third type of defect in the middle horizontal line (Perfect and defectives)

Models	ν_{zr}	RF_z (N)
No Defect	-0.73	2.41×10^1
1 unit	-0.73	2.41×10^1
2 units	-0.73	2.40×10^1
3 units	-0.73	2.39×10^1
4 units	-0.73	2.38×10^1
8 units	-0.73	2.35×10^1

Table 18: Results of ellipse-shaped structures for the third type of defect in the middle horizontal line (Perfect and defectives)

Models	ν_{zr}	RF_z (N)
No Defect	-0.73	9.22×10^1
1 unit	-0.74	9.18×10^1
2 units	-0.74	9.15×10^1
3 units	-0.73	9.11×10^1
4 units	-0.73	9.08×10^1
8 units	-0.73	8.94×10^1

Table 19: Results of peanut-shaped structures for the third type of defect in the vertical line (Perfect and defectives)

Models	ν_{zr}	RF_z (N)
No Defect	-0.73	2.41×10^1
1 unit	-0.73	2.40×10^1
2 units	-0.72	2.38×10^1
3 units	-0.72	2.36×10^1
4 units	-0.72	2.35×10^1
5 units	-0.71	2.33×10^1
6 units	-0.71	2.32×10^1

Table 20: Results of ellipse-shaped structures for the third type of defect in the vertical line (Perfect and defectives)

Models	ν_{zr}	RF_z (N)
No Defect	-0.73	9.22×10^1
1 unit	-0.73	9.13×10^1
2 units	-0.73	9.09×10^1
3 units	-0.73	9.04×10^1
4 units	-0.73	9.00×10^1
5 units	-0.73	8.95×10^1
6 units	-0.73	8.91×10^1

The third defect type does not affect both peanut-shaped and ellipse-shaped geometries. Rises and decreases in auxetic property and reaction force behavior are too small to give a remark, so it can be said that the manufacturer does not have to control this kind of defect while printing.

While printing these peanut-shaped and ellipse-shaped tubular structures, defect type four can be experienced easily because of dimensions. The length of the models is higher than two times the diameters, and their wall thicknesses are thin according to their diameter. If the part is printed through its z-direction, the result of peanut-shaped and ellipse-shaped potential defects is given in Tables 21 and 22. The effect of this defect for both geometries is increasing the auxetic property and decreasing the reaction forces at the base. So, it positively impacts structures for the auxetic property-to-stiffness ratio.

Table 21: Results of peanut-shaped structures for the fourth type of defect when printed in the z-direction (Perfect and defectives)

Models	ν_{zr}	RF_z (N)
No Defect	-0.73	2.41×10^1
0.1 mm	-0.74	2.41×10^1
0.5 mm	-0.78	2.40×10^1
1.0 mm	-0.86	2.37×10^1
2.0 mm	-0.95	2.21×10^1

Table 22: Results of ellipse-shaped structures for the fourth type of defect when printed in the z-direction (Perfect and defectives)

Models	ν_{zr}	RF_z (N)
No Defect	-0.73	9.22×10^1
0.1 mm	-0.75	9.17×10^1
0.5 mm	-0.78	9.14×10^1
1.0 mm	-0.84	9.04×10^1
2.0 mm	-0.92	8.61×10^1

Finally, as the last result, if the manufacturer prints the body in the y or x direction, it may have an ellipse cross-section. The result of this defect is shown in Tables 23 and 24 for peanut and ellipse shapes. From the tables, the geometries are not sensitive to this defect.

Table 23: Results of peanut-shaped structures for the fourth type of defect when printed in the y or x direction (Perfect and defectives)

Models	ν_{zr}	RF_z (N)
No Defect	-0.73	2.41×10^1
0.1 mm	-0.73	2.41×10^1
0.5 mm	-0.74	2.41×10^1
1.0 mm	-0.74	2.41×10^1
2.0 mm	-0.75	2.41×10^1

Table 24: Results of ellipse-shaped structures for the fourth type of defect when printed in the y or x direction (Perfect and defectives)

Models	ν_{zr}	RF_z (N)
No Defect	-0.73	9.22×10^1
0.1 mm	-0.74	9.19×10^1
0.5 mm	-0.74	9.19×10^1
1.0 mm	-0.75	9.20×10^1
2.0 mm	-0.75	9.18×10^1

From the results of the last defect, the geometry of peanut and ellipse shapes is affected when they are printed in the z-direction, but they are not sensitive to this defect when they are printed in the x or y direction. So, if the printer has some problems with the cooling or leveling of the platform and nozzle, the parts should be printed in the x or y direction.

CONCLUSIONS

In this study, the defect sensitivity of two geometries which are peanut-shaped and ellipse-shaped tubular structures is analyzed. It is supposed that they are manufactured by additive manufacturing, and from the results of this study, some preliminary manufacturing suggestions are presented.

The studied geometries have the same Poisson's Ratio and porosity value. So, under a defect condition, changes in the auxetic property or reaction forces give information about the sensitivity to the defect. Four types of defects are studied to examine the sensitivity of these geometries. The first defect was draining off extra material while printing in 3d printers. It is assumed that some holes can not be emptied due to this problem. So, some filled models are created and analyzed under 1 mm compression. From the results, both geometries are sensitive to this defect, and it does not depend on the printing direction. So, manufacturers have to solve if there is a problem like that. The second fault is the discontinuous legs of the unit cells, originating from the printer's retractions problem. This defect influences the auxetic behavior when the printing happens through the z-direction of the body, but it is not vital if the printing is in the x or y directions. So, if the printer has a retraction problem, bodies should not be manufactured in the z-direction. The reason for the third defect is the curvature shapes of the peanut and ellipse geometries. Because of their conditions and holes, filaments can not stick together while printing the long upper surfaces and flow downward. So, these regions can not carry any load. However, after analyzing this defect, it is clear that there is no substantial effect on auxetic property and reaction force values. Therefore, its impact can only be addressed if this fault causes other defects. As the last defect, the unsymmetrical dimensions of the hole structure can be examined. Changing in thickness along the z-direction may be encountered while printing in the z-direction. Also, changes in the cross-section may be seen if the body is printed through the x or y direction. Defects in the x or y directions do not increase or decrease the auxetic property and reaction forces. Still, deflection in the z-direction increases the auxetic property and reduces the reaction forces. If it is an imagined situation, the design of the parts can be done according to these outcomes, but it can be implicated that bodies are sensitive to this defect type when printed through the z-direction.

When the possibilities of realization of all defect types are equal, manufacturing through the x or y-direction is more effective than the z-direction. However, if the manufacturer knows the printer's potential, the best method can be selected according to the printer.

References

ABAQUS. *ABAQUS/Standard User's Manual*, Version 6.14, Dassault Systémes Simulia Corp, United States, 2014

Baş, H., Elevli, S. and Yapıcı, F. (2019) *Fault Tree Analysis for Fused Filament Fabrication Type Three-Dimensional Printers*, Journal of Failure Analysis and Prevention, 19, pp: 1389–1400.

Krčma, M., Paloušek, D. (2022) *Comparison of the effects of multiaxis printing strategies on large-scale 3D printed surface quality, accuracy, and strength*, The International Journal of Advanced Manufacturing Technology, 119, pp: 7109–7120.

Liu, J., Yao X., Wang, Z., Yee, J., Luan, C., He, Y. (2021) *A flexible porous chiral auxetic tracheal stent with ciliated epithelium*, Acta Biomaterialia, 124, pp: 153-165.

Peel, L., and Abdelrahman M. (2012) *Studying the Physical Properties and Auxetic Behavior of 3D-printed Fasteners*, 2012 ASEE Annual Conference and Exposition, pp: 25.1204.1-25.1204.12.

Ren, X., Das, R., Tran, P., Ngo, T.D., Xie, Y. M. (2018) *Auxetic metamaterials and structures: a review*, Smart Materials and Structures, 27, p: 023001.

Ren, X., Shen J., Tran P., Ngo T.D., Xie Y. M. (2018) *Auxetic nail: Design and experimental study*, Composite Structures, 184, pp: 288-298.

Zhang, C., Xiao, S., Qin, Q. and Wang, H. (2021) *Tunable compressive properties of a novel auxetic tubular material with low stress level*, Thin-Walled Structures, 164, p: 107882.